JOURNAL OF MATERIALS SCIENCE 18 (1983) 1213–1223

Oxidation resistance of fused TiC–C compositions containing chromium

R. N. McNALLY, P. BARDHAN
Corning Glass Works, Research and Development Laboratories, Sullivan Park, Corning, New York 14831, USA

The effect of the addition of chromium on the oxidation resistance, in air, of fused TiC–C compositions has been studied as a function of temperature, up to 1550° C. It is shown that chromium retards the oxidation principally by modifying the fused microstructure through (a) suppression of the formation of fine eutectic graphite, and (b) formation of a Cr-rich carbide case around the primary TiC. The composition and the morphology of the oxide film formed on the carbide has been characterized. It is found to consist of several regions: first, there is a dense Cr-depleted surface next to the scale-gas interface. Next, there is a porous seam with high chromium levels beneath which, and also adjacent to the bulk carbide, is another Cr-impoverished zone. The various features and their relation to the observed oxidation resistance is discussed.

1. Introduction

The microstructure of fusion-cast TiC–C for compositions with carbon > 63 at% consists of large flakes of primary graphite surrounded by an intergranular eutectic mixture of the carbide and the graphite. The process of melting and the subsequent crystallization results in what has been classified as a "natural composite" material. The virtue of the resulting microstructures was demonstrated in ZrC–C system by Rossi and Carnahan [1] and Carnahan *et al.* [2]. These authors showed that the Hasselman thermal shock damage criterion (which is proportional to the inverse of the stored elastic energy in the material) is dependent on the carbon content. It was found that hypereutectic compositions were unique in their ability to withstand high thermal stress environment [1]. In our own laboratory, extensive studies led to the development of excess graphite-containing (5 to 10 wt% excess graphite) fusion-cast carbide and carbide–boride refractory bodies [3]. Combined with the high melting points in these systems and their superior abrasion and corrosion resistance to ferrous slags, these materials would appear to have enormous potential for aerospace applications (e.g. rocket nozzles) or as heating elements or as refractories for steelmaking furnaces. In all such applications, however, there is a key property that must be satisfied by these non-oxide bodies for adequate service life without degradation of other properties; this is the oxidation resistance of the refractory. In the following we examine some of the microstructural features that govern the oxidation resistance of these ceramics.

The oxidation of TiC has been the subject of several studies [4–9]. It was reported by Watt *et al.* [5] and subsequently by Engelke *et al.* [6] that between 900 and 1000° C and in the initial stages of oxidation between 1000 and 1200° C the oxidation of TiC is linear. Munster [7] on the other hand found the oxidation to be parabolic in the 600 to 950° C temperature range. This appeared to confirm the results of Samsonov and Golubeva [8], who claimed that the rate controlling step was the diffusion of oxygen into TiC leading to the formation of the isomorphous $TiC \rightarrow Ti(C, O) \rightarrow TiO$. Stewart and Cutler [9] found that the apparent discrepancies might be related to sample geometries and surface areas. Thus powdered TiC (uncompacted) showed parabolic oxidation between 600 and 850° C; with single crystals, however, higher temperatures were required for perceptible oxidation rates and these

0022–2461/83 $03.00 + .12

single crystals appeared to oxidize at a linear rate except in the initial few minutes when it is a near parabolic rate. Similarly, using hot pressed TiC (porosity less than 3%) Lavrenko *et al.* [4] showed that between 700 and 1200° C the oxidation rate in the initial stages (up to almost 40 to 50 min) is indeed parabolic, the later oxidation (with thicker oxide films) being linear. It is worth noting that the linear oxidation period in the last two cases is associated with the appearance of rutile as the oxidation product. In addition, these authors showed that there was a transformation in the oxidation product between 400 and 600° C. Thus, for temperatures less than 600° C the anatase form of TiO_2 was found to occur whereas above 600° C the reaction product appears to be rutile. The oxide formed in the initial stage of the reaction on a compacted material is postulated to be Ti(C, O) by Lavrenko *et al.* [4] to account for the early parabolic dependence of the rate. To minimize uncertainties in the present work we have chosen (as will be shown later) to confine ourselves to (a) the linear range, that is times beyond initial parabolic dependence, and (b) temperatures where (i) oxidation is "perceptible" and (ii) there is no uncertainty about the major reaction product, namely, TiO_2 (rutile).

The presence of excess carbon in the fused cast bodies is expected to cause additional confusion. Thus, in oxidizing atmospheres at temperatures about 800° C, a significant weight loss has been reported [4] associated with the burn-out of the free carbon. The latter dominates the weight change data for temperatures at which oxidation of the carbide is insignificant. In studies on carbon steels, low alloy steels, Fe–Al alloys and austenitic steels it has been reported that carbon results in CO and is, in fact, responsible for rupturing the oxide film [10]. As might be expected then, increasing carbon content in solution in stainless steel is found to be detrimental to the oxidation resistance [11]. In their work on the oxidation of TiC, MacDonald and Ransley [12] hypothesized that the diffusion of carbon from the carbide outward through the oxide is the rate-determining step. This does not seem to be likely (q.v. [8]). While the role of carbon is not well understood, it suffices to say here that it is reasonable to expect that free carbon is expected to be more deleterious to oxidation resistance than that in solution. Thus an object of the present work was to determine the effect on oxidation resistance of decreasing free carbon. In the present study, the excess (or free) carbon is controlled by the addition of chromium to TiC. This method for controlling the dispersed carbon is described below.

The flake-like distribution of the excess carbon gives these carbides their thermal shock resistance, as discussed earlier. This morphology is primarily a consequence of the nature of the phase diagram in the Group IVB carbide systems. In these, all the carbide–carbon sections of the binary metal–carbon show simple eutectics. In the TiC–C regions, for example, the eutectic occurs at 63 ± 1 at% C at 2776 ± 6° C [13]. It has been pointed out in earlier publications [3, 14] that ternary additions which have congruent reactions with the major constituent can cause significant microstructural modifications. The ternary additive in this case is chromium. Bloom and Grant [15] have shown that there are several peritectic reactions in the Cr–C system. (In a peritectic reaction during solidification, from the molten material upon cooling, first graphite would crystallize out. The graphite reacts with the metal-rich liquid to form the carbide. Non-equilibrium phase assemblages are, therefore, typical.) In addition to expecting microstructural manipulation with chromium addition, it is hoped that, as in stainless steels, chromium would improve the oxidation resistance of the TiC–C body. This is reasonable since it is reported that the Cr-carbides have the best oxidation resistance, between 500 through to 1500° C, of all the other simple transition-metal carbides [3]. Other workers [16] have also indicated that chromium additions to TiC improve its oxidation resistance. Their data was on sintered bodies of TiC with Cr_2O_3 additions and suggests an increase in oxidation resistance only for specimens with 5 wt% Cr. With greater or less chromium additions these workers reported a decrease in oxidation resistance. Finally, there is one other reason for adding chromium to the TiC–C system. With melting points in excess of 2770° C, the binaries are not readily fusion-cast! Chromium carbides are among the lowest melting carbides with the Cr_3C_2 phase melting incongruently at about 1910° C. The expectation, therefore, was that small amounts of chromium addition would behave as the mineralizer without degrading other refractory characteristics.

In this paper we shall report on the observed changes in the microstructure of the fusion-cast

TABLE I Batched chemical composition of fused Ti–Cr–C alloys (wt%)

Alloy	Composition		
	Ti	Cr	C
A	68.6	1.7	29.7
B	66.5	4.4	29.1
C	64.4	7.0	28.6
D	63.0	8.7	28.3
E	59.5	13.0	27.5
F	56.0	17.4	26.6
G	49.0	26.1	24.9
H	42.0	34.8	23.2

TiC–C with increasing chromium addition and the related oxidation behaviour of these materials. It is shown that as chromium is added, the formation of the fine intragranular graphite is suppressed with an associated marked improvement in oxidation resistance.

2. Experimental procedure

Several test compositions were produced by melting premixed batches of the required amounts of titanium, chromium and carbon black in a 175 KW-10 KC Inductotherm induction furnace with a graphite susceptor. (For details of the equipment, see [17].) In forming the ingot of an alloy composition, graphite crucibles of various sizes were used. All fused ingots were furnace cooled. (Spectrographic analyses of the starting titanium and chromium are as follows: titanium (A. D. MacKay and Co.) > 30 wt %, iron 1.0 to 3.0 wt %, magnesium 0.1 to 3.0 wt %, silicon 0.03 to 0.1 wt %, and chromium (Fischer Scientific) > 30 wt %, iron 0.3 to 1.0 wt %. Of these impurities, iron does show up as an impurity in the oxidation product but its effect has not been analysed in the present work.)

Table I is a list of the compositions as batched. Excess graphite, about 10 vol% is picked up by the melt from the container. The compositions of the materials were analysed using wet chemical analyses, X-ray fluorescence and in some cases by modal techniques [3].

In order to determine the relative oxidation resistance 0.6 cm sample cubes were placed in a gas–oxygen furnace at 1550° C for 5.5 h. After the test, the average coating thickness was measured with a travelling microscope and an X-ray diffraction pattern was recorded to obtain the relative amount of conversion to the oxide. In addition, to ensure that oxidation rate and time were roughly in the linear range, a one centimetre cube of one composition was weighed, placed on a platinum holder and put in an electric furnace at 1000° C (with air atmosphere). The sample was weighed after various holding times. The oxidized film was examined using optical and scanning electron microscopy and the composition of the oxide film was determined using the electron microprobe.

3. Results and discussion

3.1. Fused microstructure

As suggested in Section 1, it was found that chromium indeed has a profound effect in lowering the melting points of the TiC–C alloys. With additions in the range of 4 to 7 wt % Cr, the melting points can be lowered by as much as 300° C. Accurate melting point determinations were, however, not possible because of the extreme fuming that occurs with the volatilization of chromium. (Chromium is reported [18] to have a vapour pressure of 0.5 atm at 2351° C and 1 atm at 2482° C.) The substantial loss in chromium is demonstrated by actual chemical analyses of the fused material. Fig. 1 shows the wt % Cr

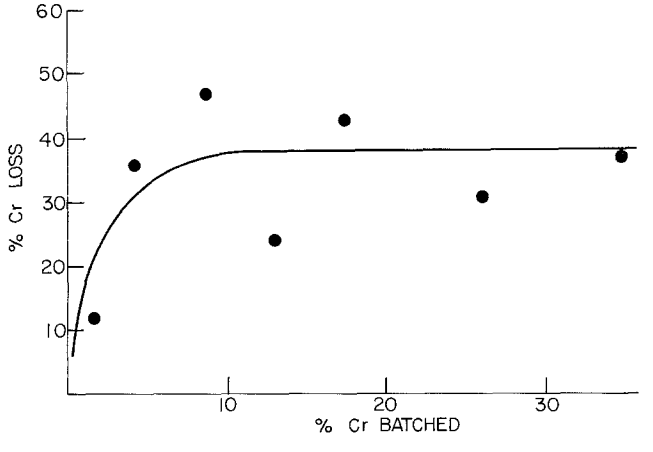

Figure 1 Relation between chromium batched and chromium lost due to volatilization during melting of compositions in the Ti–Cr–C system.

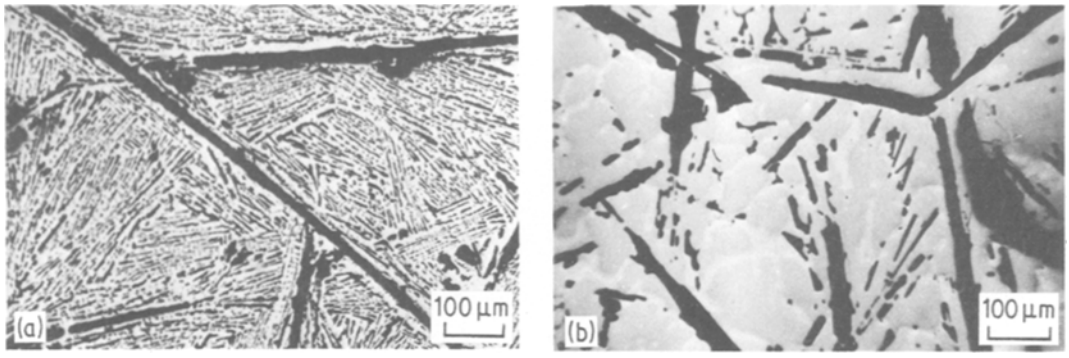

Figure 2 The effect of chromium on the microstructure of (a) hypereutectic Ti–C composition (67% Ti–33% C). (b) The presence of 9.9 wt% Cr suppresses all the secondary graphite formation. A bright Cr-rich phase can be seen to envelope a (Ti, Cr)C phase.

lost in the fused Ti–Cr–C alloy relative to the chromium batched. There is some carbon pick-up from the crucible but this has not been used to normalize the computed chromium loss as shown. The correction amounts to less than 15%. Typically, but not uniformly, between 35 to 40 wt% Cr batched is lost through volatilization during the fusion process. For this reason, in all subsequent discussion, the chromium content in the alloy is referred to in terms of the retained chromium content.

The microstructure of the fused Ti–Cr–C undergoes some dramatic changes as the chromium content increases in the body. As first shown by McNally *et al.* [3] the eutectic graphite in TiC–C, which appears as a fine dispersion between lamellae of the carbide, can be completely suppressed in the presence of chromium. The contrast in the two microstructures is shown in Fig. 2. With 9.9 wt% retained chromium, the graphite occurs predominantly as large blades. In addition to the changes in the distribution of the graphite, chromium-containing carbides begin to appear with increasing chromium addition. As a result of the persistence of non-equilibrium phases due to peritectic coring around primary crystallites extensive inhomogeneity in microstructure is observed. Up to about 4.6 wt% Cr, only a (Ti, Cr)C solid solution occurs. As the chromium content in increased to 9.9 wt%, the original solid solution appears to be encased by a higher Cr-containing carbide. (This is the highest reflectivity phase that forms an envelope around the gray, lower chromium phase in Fig. 2b.). From electron microprobe data it is estimated that there is about 4 wt% Cr in the initial (Ti, Cr)C solid solution while the Cr-rich carbide envelope contains about 44 wt% Cr. Only above approximately 25 wt% Cr is Cr_3C_2 observed in significant proportions.

3.2. Oxidation behaviour

Fig. 3 shows the oxidation rate data on a specimen containing 52.5 wt% Ti–22.5 wt% C–25 wt% Cr (estimated retained chromium about 17 wt%). It is

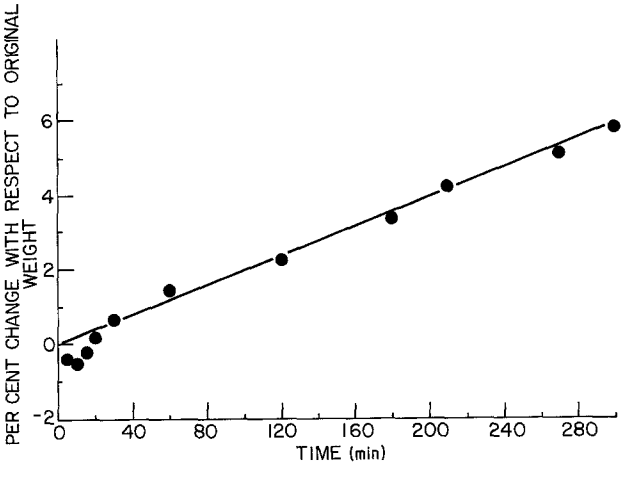

Figure 3 Oxidation behaviour, as measured by change in weight, of Ti–Cr–C at 1000° C in air. Note the observed decrease in the measured weight, referred to in the text.

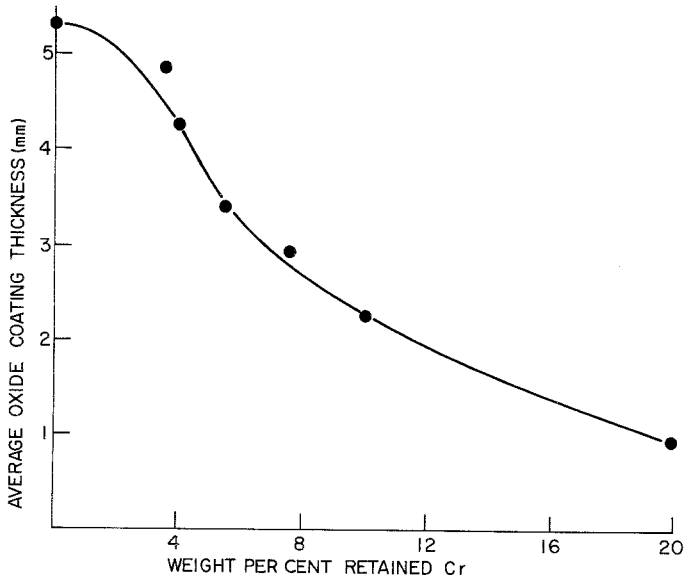

Figure 4 Measured oxide film thicknesses on Ti–Cr–C as a function of retained chromium for oxidation at 1550° C for 5.5 h.

seen that initially there is a loss in weight (up to about 20 min). This is the region where extensive burn-out of exposed intergranular graphite is believed to occur, similar to the observations of Lavrenko *et al.* [4]. There is some suggestion in the data of an initial parabolic oxidation as an oxide film forms and subsequently the material oxidizes at a linear rate. (The initial loss in weight was confirmed at a lower (4.6 wt% retained) chromium content with greater free carbon. It was found that the per cent weight loss is greater (by a factor of 2) as might be expected if it is due to the loss of the intergranular carbon.) Detailed work on kinetics of oxidation was eschewed because it was found that concurrent with the oxidation process there is considerable loss of chromium right at the oxide/gas interface. The corrections for this have a high associated uncertainty and were considered unwarranted for this study. However, for a comparison of the relative oxidation resistance of the synthesized compositions an isochronal oxidation schedule could be picked out from the data on the high chromium and the low chromium containing alloys mentioned here. For all the compositions the oxidation rate is almost linear for times greater than about 40 min with no confounding of the oxidation due to the rapid carbon burn-out. Presumably at oxidation times of say about 80 min for temperatures greater than 1000° C, the materials would behave essentially similarly (with only different rates) with the formation of rutile resulting from the oxidation of the major species. For a comparison of the oxidized microstructures the compositions were oxidized for 80 min. For a measure of the relative oxidation resistance the thickness of the oxidized film formed at 1550° C was noted. In order to ensure reasonable accuracy thick oxidation films were obtained by increasing the oxidation time to 5.5 h.

The thicknesses of the oxide scales measured (as averages of the film thickness on four sides) are shown in Fig. 4. It is clear that with additions of about 20 wt% Cr or greater there can be almost 80% improvement (as indicated by the reduction in oxide thickness) over the pure TiC–C system. The sectioned samples showing the oxide scale formation are compared in Fig. 5. In all, except

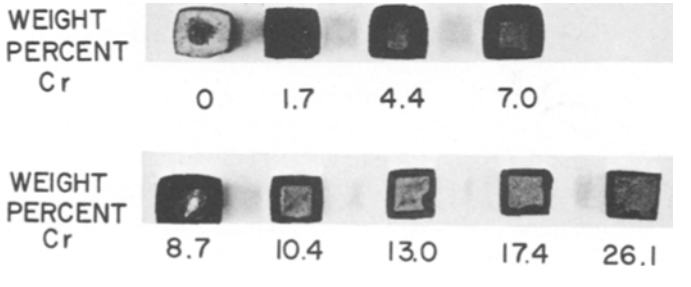

Figure 5 Cut section of several Ti–Cr–C compositions oxidized at 1550° C for 5.5 h. The cubes contain the noted amounts of chromium and the decrease in the oxide coating thickness with increasing chromium may be noted.

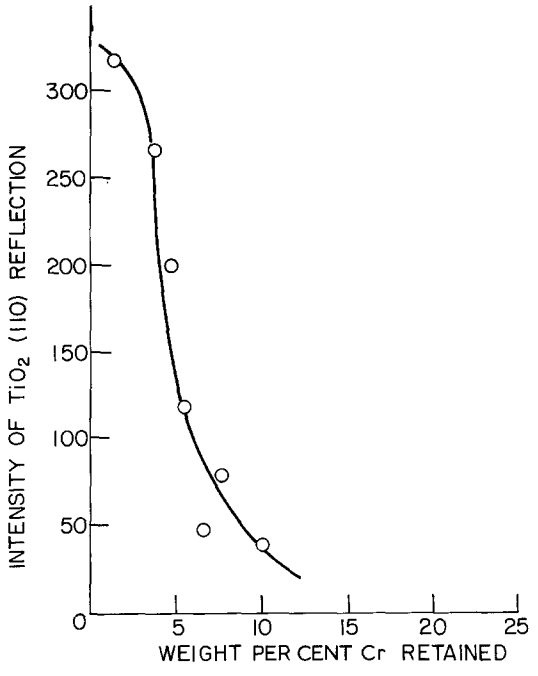

Figure 6 Diffracted intensity in arbitrary units of (110) reflection of the TiO_2 phase formed on oxidation of Ti–Cr–C compositions at 1550° C for 5.5 h as a function of chromium content.

at the lowest chromium addition, the oxide scale is adherent. Later in the discussion, we offer a tentative explanation of the anamalous oxidation of the entire sample containing 1.6 wt% Cr. The (110) X-ray diffraction peak due to the formation of rutile at the surface was also monitored on all samples. The decrease in the intensity follows the increase in chromium addition as shown in Fig. 6. This decrease is related to formation of increasing amounts of the ω-$TiO_2 \cdot Cr_2O_3$ at the expense of the rutile. X-ray diffraction of the oxidized layer is complicated by the fact that there is phase rearrangement right at the oxide–gas interface (seen later as being due to Cr_2O_3 volatilization from the surface). In any event, it appears that at low temperatures, 700° C, in addition to TiO_2, a Ti(O, C) phase, with a lattice parameter intermediate to TiO and TiC, is discernible. At higher temperatures, TiO_2 and a presumed ω-$TiO_2 \cdot Cr_2O_3$ phase can be distinguished. (The lines due to $TiO_2 \cdot Cr_2O_3$ are weak because of decrease of the content of this phase close to the surface and absorption effects for contribution to the diffracted intensity from regions deeper within the oxidized layer.)

3.3. Structure of oxide films

3.3.1. Optical microscopy

The change in the microstructure of the oxide–carbon interface as a function of temperature is shown in Fig. 7 for a composition containing about 4.6 wt% retained chromium. Little evidence of oxidation is observed at temperatures about 700° C. There is no apparent scale formation (the carbide surface, in fact, remains highly reflective) although as mentioned in the previous section Ti(O, C) is observed with some TiO_2 on the surface. Some "ghosts" due to carbon burn-out were also observed. As the temperature is increased scale formation becomes enhanced. After 1000° C, the growth of the film is linear.

The oxide film morphology also changes with temperature. At low temperatures, there is very little, if any, agglomeration of pores, rather the "ghost" of the graphite plates are clearly visible. Some pore formation is also seen right at the oxide–carbide interface where $C \rightarrow CO$ generation with the oxidation of the carbide and graphite must occur. At 1200° C, however, substantial agglomeration of the generated pores is observed. There appears to be a thin (about 25 to 50 μm) layer adjacent to the carbide, in the oxide film, that seems to contain minute porosity, whereas close to the oxide/gas interface the oxide film is quite dense and monolithic. When the temperature is raised even further, there is an inordinate thickening of the porous layer without a commensurate thickening of the denser oxide layer. Pore coarsening is observed in the dense layer at the higher temperature. This may be seen in Fig. 8.

Fig. 8 also shows the microstructural contrast in the oxide film of the low chromium and high chromium containing systems. In addition to the decrease in thickness, with increasing chromium it is found that only coarse porosity resides in the porous layer while the dense layer is essentially pore free. Graphite burn-out ghosts also appear to be absent in the high (18 wt%) chromium material.

3.3.2. Scanning electron microscopy

Two aspects of the structure of the oxide film were examined: (a) the pores adjacent to the carbide, and (b) the surface of the oxide film. From optical microscopy it had been suggested in the previous section that at 18 wt% retained chromium only coarse pores occur next to the carbide–oxide interface. Fig. 9 shows a typical feature of the porous layer, the porosity is actually

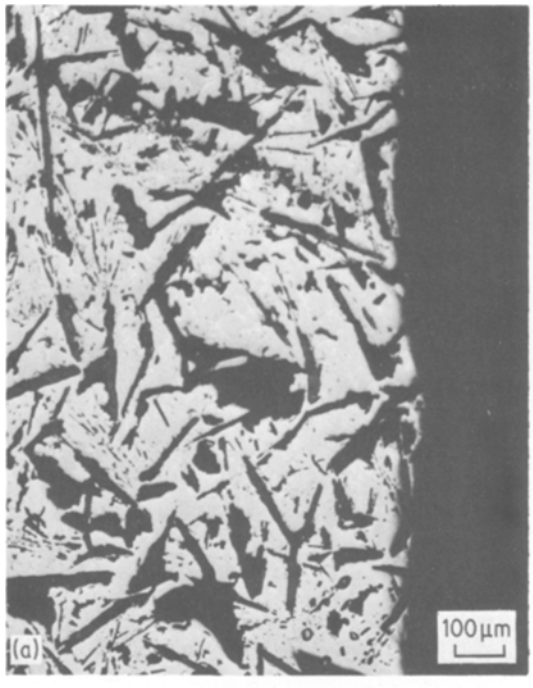

Figure 7 Optical micrograph of the carbide–oxide interface in a Ti–Cr–C composition containing 4.6 wt% retained chromium at several temperatures. Note the graphite "ghosts" next to the oxide film and the increasing pore size due to agglomeration with oxidation temperature.

continuous on a sub-microscopic scale. Scanning electron microscopy (SEM), therefore, suggests that in all carbides there is an essentially porous interfacial zone through which the gaseous products of oxidation can permeate. The difference in the low chromium and the high Cr-containing system appears to be the compactness; with increasing chromium, the porous zone is more consolidated. Coalescence of these pores occurs away from the carbide resulting in the optically observed structure.

The surface of the oxide film is not entirely featureless. Fig. 10 shows the surface of the oxide. Without the chromium addition, in TiC–C, rutile crystals (about 2.5 μm) are seen growing out of the plane of the film. Chromium additions cause these islands to be isolated (the degree to which this occurs depends on the chromium level and the oxidation temperature). The matrix consists of the finer TiO_2–Cr_2O_3 phase while the TiO_2 crystals are themselves seen to coarsen (about 4 to 5 μm). Increase in oxidation temperature leads to coarsening of the surface crystals with associated decrease in faceting as the crystals get rounded.

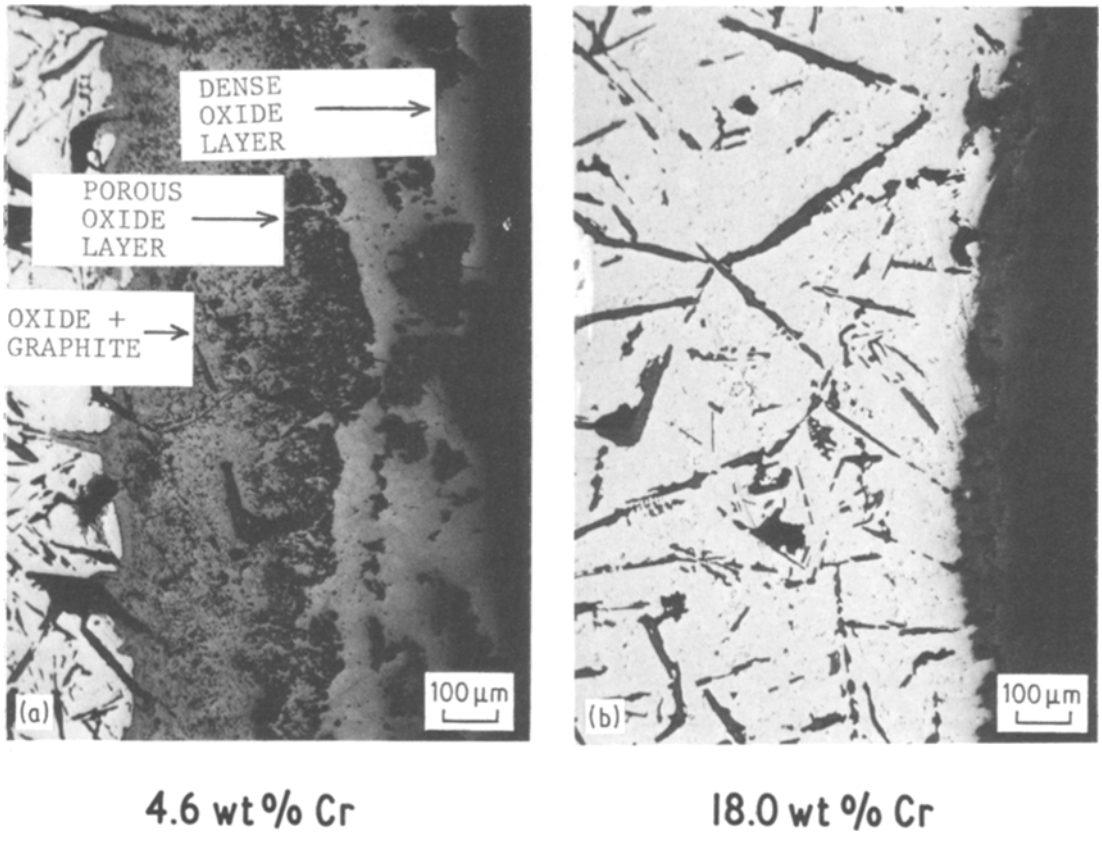

Figure 8 Optical micrographs showing the contrast in the oxidized film adhering to the surface of two Ti–Cr–C compositions oxidized in air at 1400° C for 80 min. The outer layer with some agglomerated pores is monolithic in both cases. Adjacent to this at low chromium content, there appears to be a porous layer which is separated from the carbide by a oxidized layer which still contains carbonaceous debris. No such layers are seen at 18 wt % retained chromium.

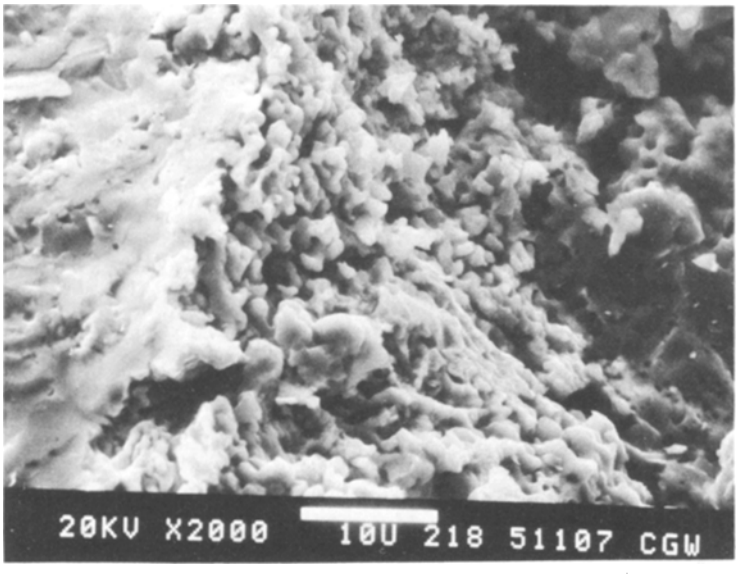

Figure 9 Scanning electron micrograph of the continuous porosity surrounding an 18 wt % Cr-containing Ti–Cr–C, oxidized at 1400° C for 80 min in air.

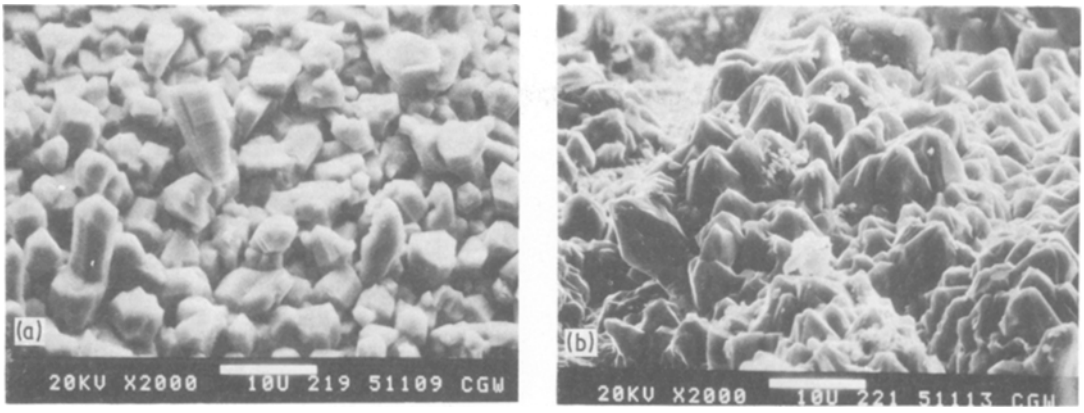

Figure 10 Surface morphology of the oxidized film on hypereutectic (a) Ti–C and (b) Ti–Cr–C (18 wt% Cr) compositions after oxidation at 1000° C for 80 min in air. Small rutile crystals are seen to grow roughly perpendicular to the oxidized surface. The addition of chromium causes some coarsening of the structure and the appearance of the secondary TiO_2–Cr_2O_3 phase.

3.3.3. Electron microprobe analysis

The composition of the oxide film and the bulk carbide close to the oxide–carbide interface is shown in Fig. 11 for a composition containing 4.6 wt% retained chromium after 80 min at 1400° C. (The discrepancy of the bulk value of chromium of about 6.8 wt% retained chromium may be due to either difference in techniques or simply the effect of the smaller sampling volume in microprobe analysis which leads to very large scatter in the data. This scatter, as seen in the data, is greatest in the crystalline bulk volume. Recall also that the microstructure is extremely inhomogeneous because of coring.) Considering the individual constituents only two features need to be noted: (a) there is depletion of chromium right near the oxide/gas interface, and (b) close to the bulk carbide and adjacent to the oxide/carbide interface there is a titanium depleted region. Since the latter region coincides with the porous layer observed earlier, the decrease is seen to be due to a lack of scattering medium. To take account of this and better assess the relative changes in the two major constituents in the oxide layer, the Cr/Ti ratios are plotted for this composition for two temperatures and shown in Fig. 12. It was found that little or no systematic deviations in the Cr/Ti ratio occurs in the scale/bulk carbide relative to the original carbide at temperatures below 1000° C; however, as the temperature is raised to 1200° C and above several zones appear with composition modulation as the oxide film is traversed. These are: (a) as mentioned above next to the scale–gas interface, a 200 to 400 μm deep region appears which is significantly impoverished in chromium. (b) Adjacent to the above and almost equal in thickness is a region that is enriched in chromium. The Cr-rich layer is bounded on either side by regions poorer in chromium so that; (c) there is another layer which is poor in chromium but characterized by a region essentially free of a concentration gradient. As observed in other chromium containing systems [19] the chromium-depleted region extends some distance (about 200 μm into the bulk carbide. Finally, (d) the bulk value of the Cr/Ti is reached about 300 μm from the scale–carbide interace.

There are clearly two factors involved in the improvement in oxidation resistance when chromium is added: (a) a physical change in the distribution of the most rapidly oxidizing phase, namely, free graphite, and (b) a chemical effect where a more oxidation resistant phase, chromium carbide is introduced.

When considering the effect on oxidation resistance of the decrease in the fine eutectic graphite it should be noted that there are three components to this: first, unlike the metal carbides the free graphite oxidizes to a disruptive vapour species without the benefit of an inhibitive oxide film formation. Second, the eutectic graphite forms an almost interconnected system of the second phase. As a consequence, it allows the penetration of the corroding atmosphere deeper into the matrix carbide. This would cause the formation of the TiC–TiO solid solution away from the scale–carbide interface leading to an "earlier" degeneration of the refractory. Third, another

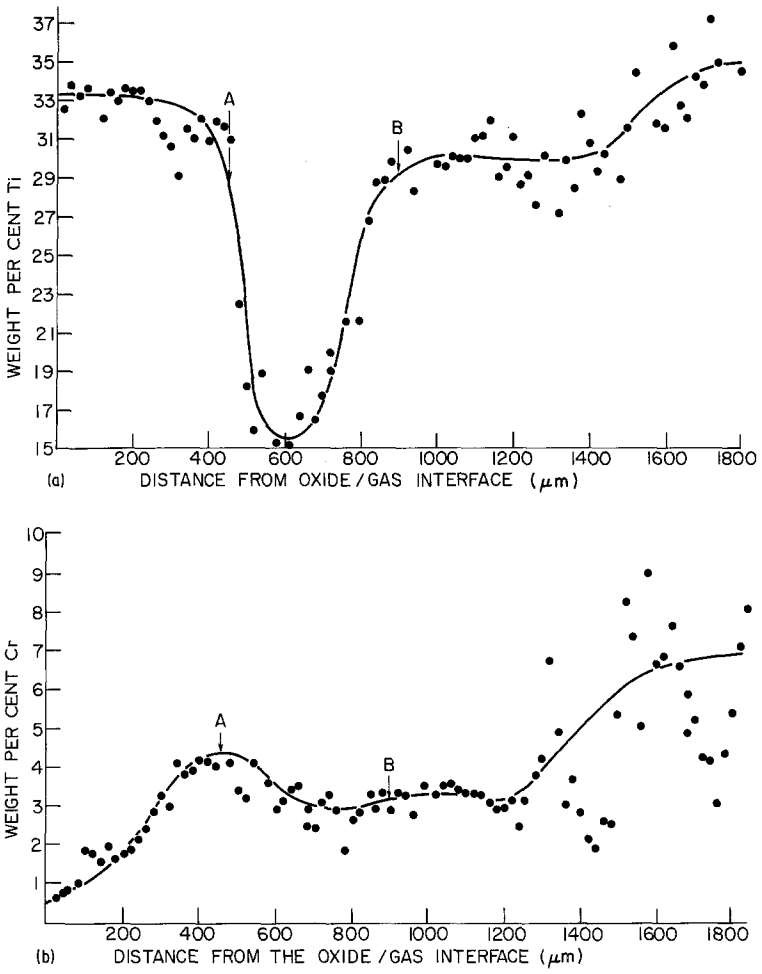

Figure 11 EMPA of the composition of the oxide film and the bulk carbide close to the oxide/carbide interface on a Ti–Cr–C composition containing 4.6 wt% retained chromium after oxidation at 1400° C for 80 min in air. (a) Titanium analysis and (b) chromium analysis. The dense oxide film extends to the point marked A. From A to B is the porous layer. The bulk carbide goes beyond and to the right of B. The scatter in titanium and chromium in the bulk carbide is due to the crystalline nature of the material with non-equilibrium coring as explained in the text.

physical change wrought by the addition of chromium is that cored crystals form at high chromium levels. The Cr-rich shell is expected to protect the high titanium interior.

Finally, an interesting feature of effect of the presence of chromium in the oxide film is the change in pore structue. While a porous layer is present in all the carbides examined it appears to be denser with increasing chromium addition. The combination of the physical factors enumerated above leads then to a more oxidation resistant product.

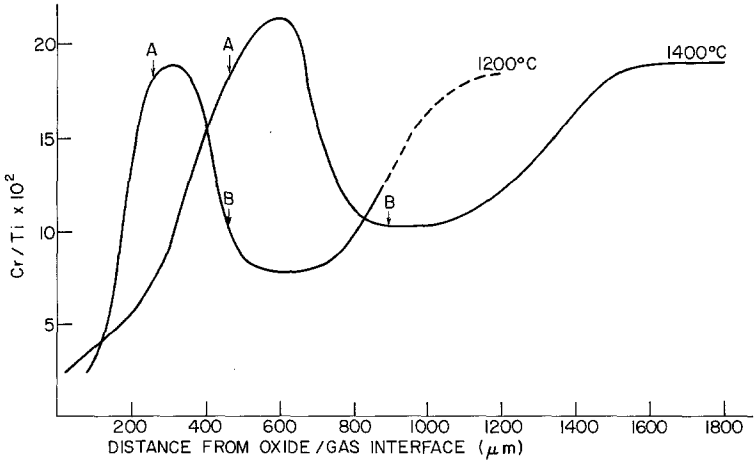

Figure 12 Profile of Cr/Ti as a function of distance from the oxide/gas interface for the oxidation of a 4.6 wt% retained chromium composition for 1200 and 1400° C in air. See Fig. 11 for explanation of markers A and B.

The chemical effects are less clear. The effect on the oxidation resistance appears to be different for low chromium additions than for high chromium additions. At low chromium levels, where there has been no modification in the dispersion of the graphite, the oxidation resistance with chromium is, in fact, worse than the Cr-free refractory. It is possible that this is due to the doping effect of chromium in the TiO_2 lattice. That is, at such low levels, chromium rather than forming a second Cr_2O_3-containing protective layer, actually produces, as implied by the Hauffe–Wagner rules [20] a more defective, more oxidation prone, n-type TiO_{2-x} oxide film, especially at the highest temperatures where ionic conductivity predominates. Although this is strictly true for only the diffusion-controlled oxidation phase a similar increase over the entire oxidation period is expected to lead to the observed degeneration of the refractory containing 1.6 wt % Cr.

As the chromium content is increased, the coupled Cr-depleted zone, Cr-enriched zone appears. These two layers appear behind the dense TiO_2 surface layer. The latter is not unexpected. That is, the lack of a protective Cr_2O_3 layer is reasonable considering the greater affinity that titanium has for oxygen than does chromium. (In the TiO_2 rich layer even at the highest chromium levels used, the higher "unvolatilized" chromium level is not expected to be greater than titanium so that a protective layer even at an early stage of the oxidation process seems an unlikely, but not impossible, event.) The appearance of the Cr-enriched section across the dense layer–porous layer interface (but dominating the porous zone) may be a consequence of kinetic factors. The occurrence of TiO, because of a large gradient in partial pressure of oxygen, P_{O_2} across the entire width of the oxide film (right up to the scale–carbide interface), ranging from atmospheric to $P_{O_2} \ll 10^{-22}$ at the latter interface, suggests that while chromium and titanium are both expected to diffuse outwards away from the interface, the lower valency cation may not diffuse as readily.

4. Conclusion

From an examination of the microstructure and the composition of the oxide film formed during the oxidation of Ti–Cr–C refractories, it is concluded that chromium retards the oxidation primarily through physical rearrangement of the constituent phases. Chromium additions inhibit the formation of fine, eutectic graphite, thereby decreasing the most readily oxidized phase. Also, chromium additions, especially at high levels form a Cr-rich core around the (Ti, Cr)C solid solution; this also helps improve oxidation resistance. The precise role of chromium in the oxidation process will, however, require more quantitative kinetic profiling of the oxide–carbide interface.

References

1. R. C. ROSSI and R. D. CARNAHAN, in "Proceedings of the Third Berkeley International Materials Conference", edited by R. M. Fulrath and J. A. Pask (John Wiley and Sons, New York, 1968) pp. 620–35.
2. R. D. CARNAHAN, K. R. JANOWSKI and R. C. ROSSI, *J. Amer. Ceram. Soc.* **52** (1969) 475.
3. A. M. ALPER, R. C. DOMAN and R. N. McNALLY, *Sci. Ceram.* **4** (1968) 389.
4. V. A. LAVRENKO, L. A. GLEBOV, A. P. POMITKIN, V. G. CHUPRINA and T. G. PROTSENKO, *Oxidation Met.* **9** (1975) 171.
5. W. WATT, G. H. COCKETT and A. R. HALL, *Metaux (Corrosion-Ind.)* **28** (1953) 222.
6. J. L. ENGELKE, F. A. HALDEN and E. P. PARLEY, Technical Report, No. WADC 59-654 , Contract No. AF 33 (616)-5888, Wright-Patterson Air Force Base, Ohio, February 1960, p. 39.
7. A. MUNSTER, *Z. Electrochem.* **63** (1959) 807.
8. G. V. SAMSONOV and N. K. GOLUBEVA, *Zh. Fiz. Khim.* **30** (1956) 1258.
9. R. W. STEWART and I. B. CUTLER, *J. Amer. Ceram. Soc.* **50** (1967) 176.
10. W. E. BOGGS, *J. Electrochem. Soc.* **118** (1971) 906.
11. T. MOROISHI, H. FUJIKAWA and H. MAKIURA, *ibid.* **126** (1979) 2173.
12. N. F. MACDONALD and C. E. RANSLEY, *Powder Met.* **3** (1959) 172.
13. E. RUDY, D. P. HARMON and C. E. BURKL, in "AFML-TR-65-2", Part 1, Vol. 2 (Air Force Materials Laboratory Metals and Ceramics Division, Wright-Patterson, Ohio, 1965).
14. P. BARDHAN and R. N. McNALLY, *J. Mater. Sci.* **15** (1980) 2409.
15. D. S. BLOOM and N. S. GRANT, *Trans. Amer. Inst. Met. Eng.* **188** (1950) 41.
16. P. SCHWARZKOPF and R. KIEFFER, "Refractory Hard Metals" (MacMillan Co., New York, 1953) pp. 44–47.
17. R. N. McNALLY, F. I. PETERS and P. H. RIBBE, *J. Amer. Ceram. Soc.* **44** (1961) 491.
18. "Metals Handbook", edited by Taylor Lyman (ASM, Metals Park, Ohio, 1948) p. 28.
19. T. HODGKIESS, G. C. WOOD, D. P. WHITTLE and B. D. BASTOW, *Oxidation Met.* **14** (1980) 263.
20. M. G. FONTANA and N. D. GREENE, "Corrosion Engineering" (McGraw-Hill, New York, 1978) p. 357.

Received 3 November 1981
and accepted 22 March 1982